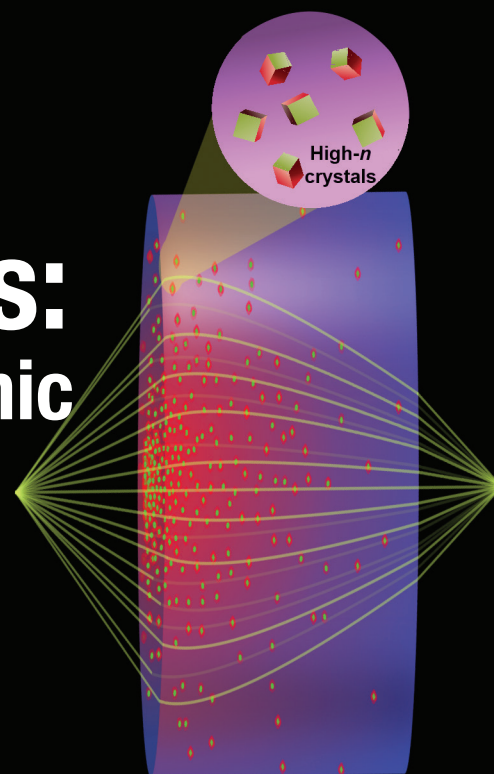# Bioinspired optics:
Chalcogenide glass-ceramic nanocomposites mark a milestone in infrared gradient refractive index materials

Credit: Kang

Infrared gradient refractive index media are realized through spatially modulated novel chalcogenide glass–ceramic nanocomposites. The gradation in color (left) corresponds to the variation in effective refractive index associated with the volume fraction of high refractive index crystals (right).

By Myungkoo Kang and Kathleen A. Richardson

A combination of multicomponent chalcogenide nanocomposites and laser/thermal processes enables a transformative opportunity to bring gradient refractive index lenses one step closer to commercialization.

Refractive optical lenses are entrenched throughout our lives.

We encounter them in our daily use of eyeglasses and camera phones as well as more advanced applications involving security and surveillance. Air, land, sea, and space-based vehicles equipped with imaging systems monitor both near and distant environments. Microscopes and telescopes employ lenses to see objects at a scale and distance far below and beyond those enabled by the human eye, respectively.

The development of these imaging systems dates to 1280 CE with the invention of eyeglasses.[1,2] Since then, researchers have made a series of breakthroughs, including the invention of the microscope in 1595 and the telescope in 1608.[1,2] However, few significant advances in lenses took place over the past century. Today's spherical lenses, made from a homogeneous medium (usually glass) with a fixed refractive index, are not appreciably different from those invented during the revolutionary era of the 1200s–1600s. While manufacturing methods have evolved from manual techniques to use of computer numerical control and precision glass molding tools, spherical and aspheric monolithic bulk optics of fixed index materials remains the fabrication strategy largely employed today.

Unfortunately, spherical lenses with uniform refractive index suffer from chromatic aberration, i.e., color distortion.[1] This distortion arises due to a material's fixed index and shape, which focuses different colors at varying physical positions in space. To solve the issue, additional corrective lenses with different shapes and refractive indices are often inserted into the optical system, as exemplified by the double-Gauss lens.[1] However, multistacked lenses typically made of high-density crystalline materials inevitably make it very challenging to minimize the size, weight, power consumption, and cost (SWaP-C) factor of entire imaging systems.

Bioinspired optics: Chalcogenide glass-ceramic nanocomposites mark a . . .
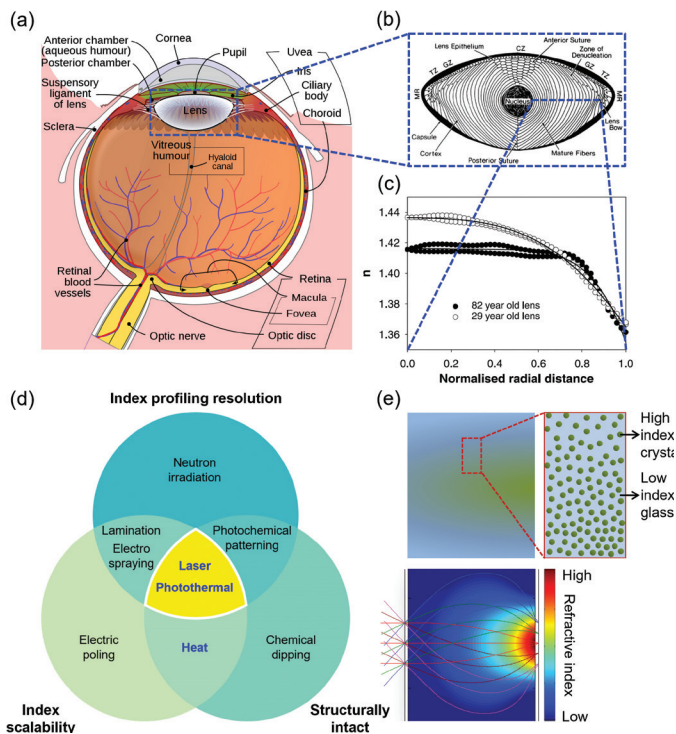

Figure 1. (a) The anatomy of a human eye. Adapted from Ref. 3 [open source]. (b) A close view of a lens in the human eye. Adapted with permission from Ref. 4, Copyright 2011 IOP Publishing. (c) The index profile of the lens. Adapted with permission from Ref. 5, Copyright 2002 Elsevier. (d) Experimental techniques to induce GRIN profiles and their assessment, and (e) A nanocomposite-based biomimetic flat GRIN lens. Credit: Kang and Richardson.

This issue is compounded in the infrared (IR) portion of the electromagnetic spectrum, where high-density single crystal materials (i.e., germanium and silicon) serve as the material of choice in legacy optical systems. The need to minimize the SWaP-C factor for multicomponent lens systems thus requires today's optical community to rethink the strategy of both material choice and form factor.

Bioinspired optics: Gradient refractive index materials

Nature often inspires efficient structural designs for man-made products. We can again rely on bioinspired examples for possible solutions to the lens distortion issue.

The microstructure of lenses within human eyes have a spatially varying mass density that correspondingly gives rise to a gradient refractive index (GRIN) ranging from 1.386 to 1.406, as illustrated in Figs. 1a–c.[3-5] The GRIN profile removes much of the chromatic aberration, allowing the eye to image with good resolution.

The significant advantages of GRIN lenses include[6-8]
1) Single component required to correct the chromatic aberration,
2) Flat or arbitrary shape,
3) Enables optical platforms with a substantially reduced SWaP-C factor as well as new design degrees of freedom, and
4) Opens previously uncharted novel optical functions.

Since Wood's pioneering work experimentally realized the creation of a man-made GRIN profile,[6] researchers proposed

a wide variety of methods to develop similar optical function in applications that span the visible and IR spectral regions.[6-8] Meanwhile, it was only during the recent two decades when technological advances first became feasible, due to the challenge of finding suitable target materials that can enable such methods.

Three key criteria of a candidate GRIN solution include the abilities to
1) Create an arbitrary GRIN profile in a 3D volume;
2) Create a GRIN profile throughout the entire volume of a target material to maximize a resulting phase shift of propagating light; and
3) Induce minimal optical and structural defects, thereby maintaining a lens' optical transparency within the component's environment of use.

Figure 1d shows a series of methods that were experimentally demonstrated and their assessments based on the aforementioned criteria. Notably, spatially controlled direct laser writing,[9] gradient heat treatment,[10] and the photothermal method (a sequential hybrid form of these two processes)[11,12] recently gained interest due to their ability to mitigate issues associated with structural defects often induced in other techniques. These issues can induce artifacts associated with interfaces from neighboring layers (lamination[13] and electro-spraying[14]), damage/modification from long-range macroscopic bombardment/diffusion of ions (neutron irradiation[15] and electro-poling[16]), and a limited diffusion-defined index modification within a near surface volume (ion exchange/chemical dipping[7] and photochemical[17]).

The photo (laser), thermal (heat), and photothermal processes use either crystallization or amorphization to convert a starting material into a nanocomposite consisting of coexisting high index crystalline phases and low index amorphous phases. The refractive index of a nanocomposite with multiple coexisting subwavelength phases can be approximated as an effective medium as formulated by $n_{effective} \approx \sum_{i=1}^{N}(V_{i_{th}} \text{ phase} \times n_{i_{th}} \text{ phase})$, where n and V correspond to the refractive index and volume fraction of each phase within a nanocomposite, respectively. The formulation assumes that spatial variation in the volume density of high index nanocrystalline phases leads to a transmissive effective medium with a GRIN profile, with low loss.

Figure 1e shows an example of such a microstructure where the number density of high index nanoparticles (green) varies spatially within a low index matrix (blue),[8] resulting in a single-component flat GRIN lens in which propagating light is guided along curved trajectories.

Candidate materials and processes

Efforts to find a material system that allows for the aforementioned microstructure/index modification processes in the IR spectral region have resulted in significant progress over the past two decades.

In 2007, researchers at the University of Rennes (France) reported that heat treatment of a bulk chalcogenide $GeSe_2$–As_2Se_3–PbSe glass could result in the formation of a glass-ceramic nanocomposites containing high index crystals.[18] Motivated by this finding, a collaborative group of teams at Clemson

Figure 2. (a) $GeSe_2$–As_2Se_3–PbSe glass' ternary compositional phase diagram at room temperature, and (b) The glass's composition-temperature phase diagram. Adapted with permission from Ref. 20, Copyright 2021 Wiley. (c) Expected microstructures of glasses with four representative compositions. Credit: Kang and Richardson. d) A summary of starting morphology-stimulation method-resulting evolution correlation. Adapted with permission from Ref. 9, Copyright 2018 OSA Publishing; Ref. 10, Copyright 2020 Wiley; and Ref. 11, Copyright 2018 Wiley. (e) Spatial composition analysis of a nanocomposite. Adapted with permission from Ref. 10, Copyright 2020 Wiley.

University (now at the University of Central Florida), The Pennsylvania State University, and Lockheed Martin Corporation extended this study to show how direct laser writing, heat treatment, or a hybrid process could be used as a versatile, scalable, and tailorable method enabling spatial refractive index modification of chalcogenide glass matrices in both bulk and thin film forms.[6,8–12,19,20]

Understanding why the material system is suitable for the specific types of external stimuli and is uniquely poised as a promising GRIN medium candidate requires a close look at the glass's phase diagram. Figures 2a and 2b show horizontal and vertical components of the $GeSe_2$–As_2Se_3–PbSe bulk material's phase diagram, respectively.[10,19,20]

Following a rapid quenching of a melted compound, the chalcogenide glass's resulting room temperature microstructure is composition-dependent, as indicated by the glass-forming and crystal-forming regions in the horizontal ternary phase diagram. Resulting materials with compositions on the crystal-forming region exhibit randomly distributed crystals with a large size distribution, whereas those on the glass-forming region can show a well-defined composition-dependent microstructural evolution. Specifically, the vertical composition–temperature phase diagram is constructed along the dotted blue line drawn within the glass-forming region on the horizontal diagram.

A prominent feature in the vertical phase diagram is an immiscibility dome spanning over compositions ranging from about 10–45 mol% of PbSe at room temperature.[8] The immiscibility dome indicates that an increase in PbSe content involves microstructural transitions from a homogeneous medium (~0–10 mol% PbSe) to a nanocomposite medium consisting of lead-rich particles in a lead-deficient matrix (~10–30 mol% PbSe) to a nanocomposite medium consisting of lead-deficient particles in a lead-rich matrix (~30–45 mol% PbSe) back to a homogeneous medium (~45–50 mol% PbSe). The four blue stars correspond to representative compositions in each regime, and their expected microstructures are illustrated schematically in Fig. 2c.
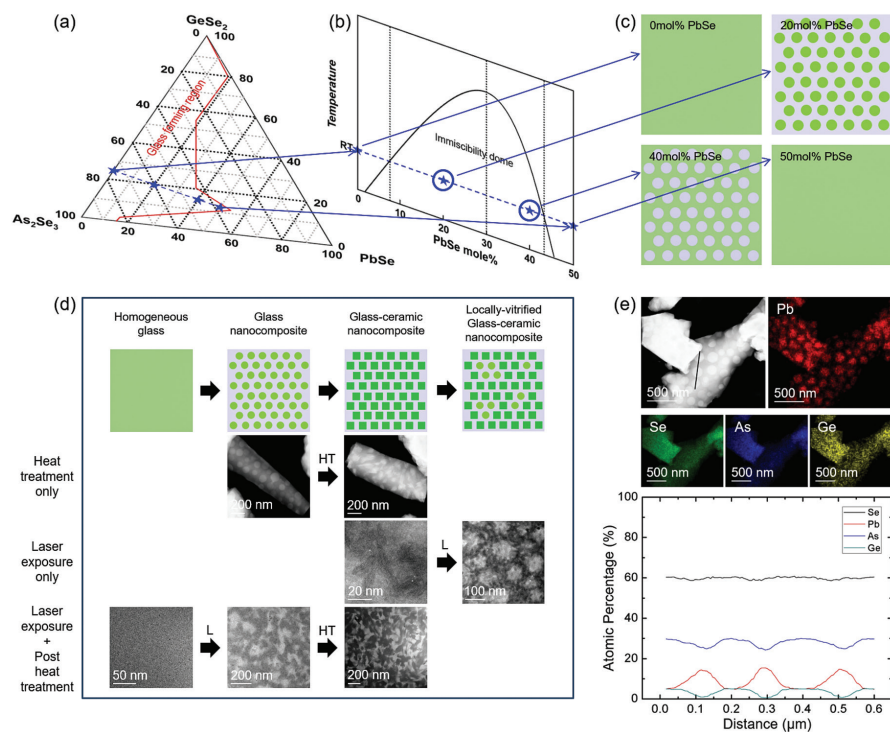
Here, nanocomposites with a composition within the immiscibility dome are of particular interest as a starting point toward a candidate GRIN material. Within these regions, the Pb-rich phases existing as either particles (~10–30 mol% PbSe) or a matrix (~30–45 mol% PbSe) in the starting glassy nanocomposites are inherently unstable and prone to crystallization while their counterpart lead-deficient phases remain amorphous upon heat treatment. The exclusive crystallization of lead-rich phases induces the formation of high index $Ge_{0.1}Pb_{0.9}Se$ (~10–30 mol% PbSe) or PbSe (~30–45 mol% PbSe) nanocrystals with indices far greater than those of a coexisting lead-deficient amorphous phase and other induced crystals.[10,19] The lead-rich phases in the starting nanocomposites are uniformly dispersed/sized and their average size is orders of magnitude smaller (at most up to ~200 nm) than the wavelength of IR light.[10,19,20] These characteristics allow the effective refractive index of the nanocomposite to increase while it remains as a low-loss transmissive effective medium in the IR upon heat treatment.

Meanwhile, inspired by phase change materials, an alternative approach was used to induce a reverse transition from a glass-ceramic back to a glassy state.[9] The rationale behind this approach is that a spatial control of the degree of crystallization within a starting glass-ceramic matrix would lead to a local decrease in refractive index, thereby creating a GRIN structure. The method would not only switch between extremes in fully crystalline and amorphous states, but it would also reach intermediate states, thereby allowing a fine control of refractive index within a material. The process uses precisely controlled laser irradiation to melt the glass-ceramic, thereby re-amorphizing the local region and reversing the cumulative extent of crystallization. The amorphization is spatially controlled by the fluence and movement of the laser writing process, representing how the term laser-induced vitrification (LIV) was coined by our team.[9]

As chalcogenide $GeSe_2$–As_2Se_3–PbSe glasses in a thin film form undergo a thermal history vastly different from that of a bulk solid, such processing results in mor-

phologically homogeneous media across a wide range of compositions.[11,12] This difference is directly associated with their typical deposition technique. In efforts by our team, chalcogenide films are deposited predominantly using thermal evaporation where evaporated source materials experience excessively fast cooling as they are deposited on a substrate maintained at either room or a cold temperature. As a result of the process, the source materials are instantaneously frozen into a highly metastable amorphous phase. Because there is no time for constituent atoms/molecules to rearrange during the fast condensation process, their resulting morphology exhibits that of the "parent" vapor phases. As the medium is homogeneous, this situation necessitates a different strategy to functionalize the material toward a GRIN medium.

The highly metastable, homogeneous films have a strong tendency to separate into lead-rich and lead-deficient phases at an activation energy lower than that required for as-quenched bulk glasses. Meanwhile, the facile phase transformation comes with a caveat. Relying only on heat treatment would induce the spontaneous formation of crystals with a large size distribution. Crystallites with sizes in the upper part of the size distribution, outside the effective media approximation's regime, are likely to scatter incident IR light, leading to optical loss. Also, their random spatial and size distributions leave none to very little controllability over the formation of GRIN profiles.

To overcome the challenge, direct laser writing was introduced and sequentially combined with heat treatment.[11,12] The rationale behind an addition of the laser process includes

1) It activates the process whereby a starting homogeneous film can be separated into lead-rich and lead-deficient glassy phases;

2) Tunability of the magnitude and location of phase separation by controlling fluence and laser exposure;

3) Post heat treatment of the laser-induced nanocomposite allows energetically unstable lead-rich phases to be exclusively converted into high index crystals while keeping the lead-deficient

low index phases glassy at a temperature lower than that required for a heat treatment-only condition; and

4) The size of the high index crystalline phases within the resulting glass-ceramic film is small and narrowly distributed, allowing the nanocomposite to remain transparent.

This approach enables GRIN layers to be applied to bulk spherical optics, thereby creating aspheric optical functions. Such an approach can result in considerable cost savings in the manufacturing process.

The three representative cases discussed above indicate that a specific choice of post stimulation process suitable for the realization of GRIN media is largely determined by the starting medium's morphology (phase separated or homogeneous) and microstructure (glassy or glass-ceramic). The starting morphology-stimulation method correlation is summarized in Fig. 2d. Here, the top row illustrates morphological/microstructural transitions that the material system can undergo: from i) a homogeneous glass to ii) a glass nanocomposite to iii) a glass-ceramic nanocomposite to iv) a partially vitrified glass-ceramic nanocomposite.

No matter where the starting point is, a key requisite for the realization of GRIN media is to convert a starting morphology into a glass-ceramic nanocomposite consisting of small (sub-100 nm) monosized high index crystallites within a low index glassy phase. The transmission electron microscope images in Fig. 2d summarize how three post-stimulation processes including heat treatment-only, laser-only, and a hybrid of these two processes (i.e., photo-thermal process) are coupled with the specific starting stages of target materials and induce them to evolve into glass-ceramic media.[9–12,19,20]

Figure 2e shows a TEM image and corresponding X-ray energy dispersive spectroscope maps collected from a nanocomposite with 20 mol% PbSe as a representative composition within the material system's immiscibility dome.[10] The presence of phase separation into lead-rich particles and a lead-deficient matrix is clearly indicated by the red map corresponding to lead. To quantify the extent of phase separation, the atomic

percentages of four constituent elements were extracted along the black line in the TEM image. The spatial profiles in Fig. 2e show how each element's quantity varies over the distance across particle and matrix regions, highlighting a large difference in local atomic percentages of lead in particle and matrix regions.

Refractive index modifications

How the microstructural/morphological evolution leads to changes in the composite's refractive index is presented for heat treatment-only (Figs. 3a–c), photo-thermal (Figs. 3d–f), and laser-only processes (Figs. 3g–i). The heat treatment of bulk glasses converts them into glass-ceramics whereby the type and volume fraction of each crystalline phase is dictated by the composition of the parent glasses, as shown in Fig. 3a.[10]

It is important to note that the volume fraction of lead-containing crystalline phases (either $Ge_{0.1}Pb_{0.9}Se$ or PbSe) increases with lead content of starting glasses. Because the refractive indices of these phases in the mid-wave IR for $Ge_{0.1}Pb_{0.9}Se$ (4.81) and PbSe (4.90) crystals are far greater than those of As_2Se_3 (2.41), selenium (2.65) crystals as well as the parent glass matrices (nominally around 2.48) at a wavelength of 4.515 μm as an example, the lead-containing crystals are clearly responsible for an increase in effective refractive index upon conversation of glasses into glass-ceramics.[10] The impact of starting composition and heat treatment on an increase in effective refractive index of nanocomposites is summarized in Fig. 3b, highlighting an ability to target a specific index through a specific choice of "knobs" of the composition and thermal processing.[10] Also, Fig. 3c shows that while there is an optical loss in the short-wave IR originated from scattering of incident light at interfaces between high index crystals and a low index matrix, the nanocomposite media still retain their mid-wave IR transparency upon glass to glass-ceramic conversion.

Figures 3d and 3e show an example of such index tailorability via a photo-thermal process carried out on films.[9] Specifically, an increase in laser exposure fluence followed by a fixed heat treatment protocol leads to a greater volume

fraction of lead-containing high index nanocrystals, thereby increasing the effective refractive index of films, as shown in Fig. 3d.[11] Figure 3e shows the extensive impact of laser exposure fluence on a net change in index of films reaching about 0.08 with respect to those with no laser exposure at a wavelength of 4 μm.[11] The well-defined monotonic relationship serves as a "design curve" that quantifies a specific laser exposure fluence required to induce a target index change. Further to the controllability of index and the maintenance of optical transparency upon glass to glass-ceramic conversion, it is imperative to test whether a GRIN structure minimizes a chromatic aberration of an optical media, as one of the key promised benefits for the employment of GRIN. We assume a radial GRIN structure where its effective refractive index continuously varies over the range shown in Fig. 3d. We then extract a GRIN Abbe number of the medium.[11] Figure 3f shows the magnitude of Abbe numbers for the radial GRIN medium and compares the values with those for its homogeneous counterparts as well as other materials over three spectral ranges of short-wave IR, mid-wave IR, and long-wave IR. Materials that are less dispersive and correspondingly lower chromatic aberration have a greater magnitude of Abbe number. The orders of magnitude increase in the absolute value of the GRIN Abbe number observed in Fig. 3f indicates that the GRIN medium should experience far less chromatic aberration than its counterpart homogeneous medium.

Figs. 3g–i.[9] present the ability to locally tailor the effective refractive index using a laser-only process. Figure 3g shows an array of laser-written structures and corresponding Raman spectra collected from three locations on (A), near (B), and away from (C) a pillar.[9] The clear differences in their spectral features indicate the different extents of laser-induced vitrification.

To quantify the extent of vitrification in each region, the spectra in Fig. 3g are compared to those collected from a starting glass-ceramic (i.e., no vitrification) and a glass (i.e., a complete vitrification) in Fig. 3h.[9] Because the two reference states in Fig. 3h correspond to specific
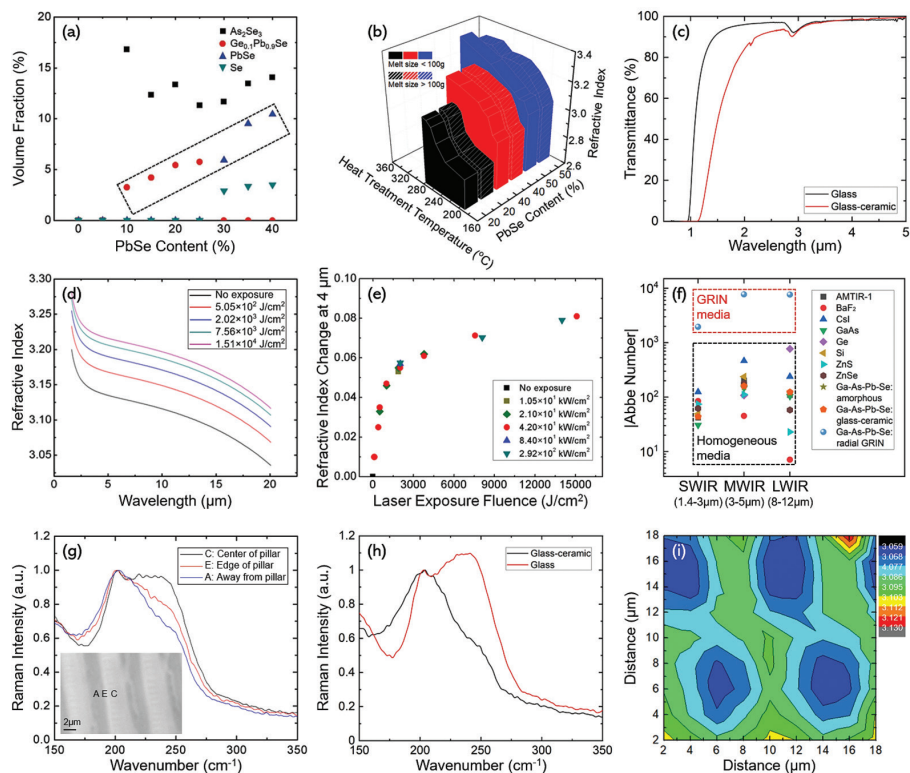

Figure 3. (a) Types of crystalline phases formed upon heat treatment of bulk materials, and (b) A starting composition-heat treatment temperature-resulting refractive index correlation for bulk materials. Adapted with permission from Ref. 10, Copyright 2020 Wiley. (c) The heat treatment-induced evolution of transmittance for a bulk material. Credit: Kang and Richardson. The impact of laser dose on (d) index dispersion of thin films and (e) index changes of thin films at a wavelength of 4 μm, and (f) Abbe numbers of various homogeneous and GRIN media. Adapted with permission from Ref. 11, Copyright 2018 Wiley. (g) Raman spectra of glass and glass-ceramic materials; (h) Raman spectra collected from regions on, near, and away from a laser-vitrified pattern within a glass-ceramic material; and (i) A corresponding Raman-converted index map on the surface of the material. Adapted with permission from Ref. 9, Copyright 2018 OSA Publishing.

effective indices, the quantitative comparison of the spectra in Figs. 3g and 3h allows us to extract the effective refractive indices of three local regions where the spectra in Fig. 3g were collected.

Based upon this approach, Raman spectra collected from multiple locations over a large area are converted into a map of effective refractive index, as shown in Fig. 3i.[9] Each blue "chain" corresponds to each laser-written structure where the lateral succession of circular features represents the movement of a laser spot to write such an array. Importantly, the indices of laser-written arrays are lower than those outside the regions, showing the ability to spatially tune effective refractive index within a single optical medium.

Realization of GRIN structures

The process–structure–property relationships defined for the three approach-

es were used to create functional optical media with specifically programmed GRIN profiles in both radial and axial directions. As an example of a GRIN profile created within a bulk specimen using a thermal-only process, the inset in Fig. 4) illustrates a 50 mm-long rod that underwent a gradient heat treatment where the specimen experienced spatially varying temperatures from 225°C at the left cold end to 260°C at the right hot end.[10] We sliced a resulting glass-ceramic rod into multiple discs and measured refractive indices for four representative discs. Figure 4a shows that a disc whose original location is closer to the hot end exhibits a greater index, indicating the formation of an axial GRIN profile within the bulk rod specimen.[10]

Meanwhile, the photothermal process offers spatially more options thanks to the versatility and spatial resolution of the laser beam's movement. The laser
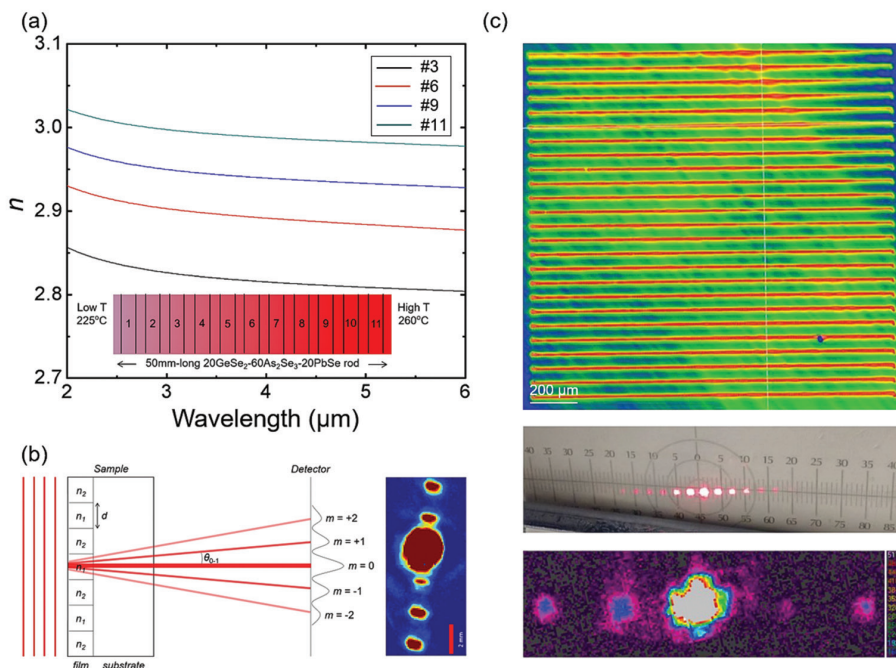
Figure 4. (a) A 50 mm-long rod subjected to a gradient heat treatment and corresponding refractive indices collected from various slices from the rod. Adapted with permission from Ref. 10, Copyright 2020 Wiley. (b) Arrays of photothermally-induced glass-ceramic patterns within a glass thin film functioning as a diffraction grating. Adapted with permission from Ref. 11, Copyright 2018 Wiley. (c) Arrays of laser-vitrified patterns within a bulk glass-ceramic matrix functioning as a diffraction grating in both reflection and transmission modes. Adapted with permission from Ref. 9, Copyright 2018 OSA Publishing.

exposure, which is the first stage of the two-step process, can be done with an optical mask as well. For example, we used an optical mask that allows laser beams to reach the surface of a film in a laterally discrete fashion, where the film has alternating laser-exposed and unexposed regions. Subsequently, the film underwent a heat treatment to convert the laser-exposed regions into glass-ceramics while the laser-unexposed regions remained glassy, which led to formation of a grating with spatially alternating high and low index regions.

Figure 4b illustrates the grating structure we fabricated and shows diffraction spots created at a detector with the transmission of 2 μm laser light through the structure.[11] The diffraction spots can be used to extract a difference in indices of laser-exposed and unexposed regions within the grating structure. The index change is extracted to be 0.077 for the specific case in Fig. 4b and closely matches a value of 0.08, which was targeted based on a specific choice of laser exposure and post heat treatment parameters.[11]

The formation of a grating structure was also realized using a spatially modulated LIV (i.e., laser-only) process on a bulk glass-ceramic specimen, as shown in Fig. 4c.[9] The LIV-induced structure subjected in transmission (λ = 2 μm) and reflective (λ = 0.632 μm) modes leads to the generation of spots, confirming the functionality of the structure as a grating. An extracted difference in indices of laser-vitrified glassy and unexposed glass-ceramic regions within the grating structure is –0.056. The value is consistent with a change (–0.062) extracted from the Raman-converted index map of gratings in Fig. 3i.[9] Therefore, three examples demonstrated in Figs. 4a–c confirm that thermal-only, photothermal, and laser-only processes are capable of creating GRIN structures with spatially and optically great precisions.

Remaining challenges and outlooks

While the work reported here focused on a specific chalcogenide material system to demonstrate how glass science can be used to design new optical mate-

rials with diverse functions, the premise whereby low-loss nanocomposites can be created to yield tunable optical functions in a thin and/or flat form factor is an attractive approach to enable more compact optical components and systems. We have just begun to explore a small fraction of this chalcogenide material's phase diagram, and much of its further potential has yet to be discovered.

Along the way, key information to identify the medium's resulting phases as well as their size, shape, volume fraction, connectivity, and composition is needed because these factors collectively determine the medium's resulting optical performance. Such information is vital to construct a predictive quantitative process–structure–property relationship that can serve as a "look-up table of processing metrics" for the realization of optical components with target optical behavior. Meanwhile, a challenge to identify the microstructure of this material system still leaves us room for improvement. Specifically, widely used TEM has an intrinsic limitation to characterize its microstructure in a 3D space due to its 2D projection method where coexisting phases are often seen overlapped or partially revealed. Also, the material is substantially sensitive to ion irradiation, making it challenging to prepare destruction/contamination-minimized cross-sectional TEM specimens during an ion beam-assisted milling process. Additionally, optical characterization methods to accurately measure arbitrary GRIN profiles still require further improvement to see such an optical function in actual discrete components.

As one feasible solution, atom probe tomography (APT) has gained interest in the optical materials community due to its ability to identify the microstructure and chemistry of target specimens in a reconstructed 3D volume.[20] In addition, the metrology method allows high spatial resolution and high detection sensitivity to be achieved simultaneously, thereby overcoming the trade-off relationship that is well known for other micro- and nanoscale analytical instruments.

To better understand the chalcogenide nanocomposites' microstructures and

chemistries, endeavors to optimize parameters for both focused ion beam-assisted APT specimen preparation and data collection are in progress.[20] Especially, we foresee that by using plasma- or cryo-focused ion beam, undesirable ion-matter interactions beyond intended milling, which often induce microstructural defects, can be minimized during an APT tip preparation stage, thereby allowing APT to retain 3D data as close as that of an original specimen.

Findings from the spatially improved microstructural analysis combined with enhanced optical metrology tools for GRIN characterization will not only reveal further insight into the material system's response to laser and thermal treatments, but it will also refine the predictive quantitative process–structure–property relationship, facilitating the design, fabrication, and expanded use of GRIN optical components.

About the authors

Myungkoo Kang and Kathleen A. Richardson are research scientist and professor, respectively, in CREOL, the College of Optics and Photonics at the University of Central Florida. Contact Kang at myungkoo@creol.ucf.edu and Richardson at kcr@creol.ucf.edu.

References

[1] E. Hecht, *Optics*, Addison-Wesley, Reading, MA **1998**.

[2] G. Zuccarello, D. Scribner, R. Sands, and L. J. Buckley, "Materials for bio-inspired optics," *Adv. Mater.* **14**, 1261 (2002).

[3] https://en.wikipedia.org/wiki/Iris_(anatomy)#/media/File:Schematic_diagram_of_the_human_eye_en.svg (Wikipedia page for Human eye, Open source, Accessed in **June 2021**).

[4] P. Nogueira, M. Zankl, H. Schlattl, and P. Vaz, "Dose conversion coefficient for monoenergetic electrons incident on a realistic human eye model with different lens cell populations," *Phys. Med. Biol.* **56**, 6919 (2011).

[5] B. A. Moffat, D. A. Atchison, and J. M. Pope, "Age-related changes in refractive index distribution and power of the human lens as measured by magnetic resonance micro-imaging in vitro," *Vision Res.* **42**, 1683 (2002).

[6] J. Teichman, J. Holzer, B. Balko, B. Fisher, and L. Buckley, *Gradient Index Optics at DARPA*, The Institute for Defense Analyses, Alexandria, VA **2014**.

[7] D. T. Moore, "Gradient-index optics: a review," *Appl. Opt.* **19**, 1035 (1980).

[8] K. Richardson, M. Kang, L. Sisken, A. Yadav, S. Novak, A. Lepicard, I. Martin, H. Francois-Saint-Cyr, C. M. Schwarz, T. S. Mayer, C. Rivero-Baleine, A. J. Yee, and I. Mingareev, "Advances in infrared GRIN materials: a review," *Opt. Eng.* **59**, 112602 (2020).

[9] M. Kang, L. Sisken, J. Cook, C. Blanco, M. C. Richardson, I. Mingareev, and K. Richardson, "Refractive index patterning of infrared glass ceramics through laser-induced vitrification," *Opt. Mater. Express* **8**, 2722 (2018).

[10] M. Kang, L. Sisken, C. Lonergan, A. Buff, A. Yadav, C. Goncalves, C. Blanco, P. Wachtel, J. D. Musgraves, A. V. Pogrebnyakov, E. Baleine, C. Rivero-Baleine, T. S. Mayer, C. G. Pantano, and K. A. Richardson, "Monolithic chalcogenide optical nanocomposites enable infrared system innovation: Gradient refractive index (GRIN) optics," *Adv. Opt. Mater.* **8**, 2000150 (2020).

[11] M. Kang, A. M. Swisher, A. V. Pogrebnyanov, L. Liu, A. Kirk, S. Aiken, L. Sisken, C. Lonergan, J. Cook, T. Malendevych, F. Kompan, I. Divliansky, L. B. Glebov, M. C. Richardson, C. Rivero-Baleine, C. G. Pantano, T. S. Mayer, and K. Richardson, "Ultra-low dispersion multicomponent thin film chalcogenide glass for broadband gradient index optics," *Adv. Mater.* **30**, 1803628 (2018).

[12] I. Mingareev, M. Kang, M. Truman, J. Qin, G. Yin, J. Hu, C. M. Schwarz, I. B. Murray, M. C. Richardson, and K. A. Richardson, "Spatial tailoring of the refractive index in infrared glass-ceramic films enabled by direct laser writing," *Opt. Laser Technol.* **126**, 106058 (2020).

[13] D. Gibson, S. S. Bayya, V. Q. Nguyen, J. D. Myers, E. F. Fleet, J. S. Sanghera, J. Vizgaitis, J. P. Deegan, and G. Beadie, "Diffusion-based gradient index optics for infrared imaging," *Opt. Eng.* **59**, 112604 (2020).

[14] S. Novak, P. T. Lin, C. Li, C. Lumdee, J. Hu, A. Agarwal, P. G. Kik, W. Deng, and K. Richardson, "Direct electrospray printing of gradient refractive index chalcogenide glass films," *ACS Appl. Mater. Interfaces* **9**, 26990 (2017).

[15] P. Sinai, "Correction of optical aberrations by neutron irradiation," *Appl. Opt.* **10**, 99 (1971).

[16] L. Karam, F. Adamietz, D. Michau, C. Goncalves, M. Kang, R. Sharma, G. S. Murugan, T. Cardinal, E. Fargin, V. Rodriguez, K. A. Richardson, and M. Dussauze, "Electrically polarized amorphous sodo-niobate film competing with crystalline lithium niobite second order optical response," *Adv. Opt. Mater.* **8**, 2000202 (2020).

[17] C. M. Schwarz, S. M. Kuebler, C. Rivero-Baleine, B. Triplett, M. Kang, Q. Altemose, C. Blanco, K. A. Richardson, Q. Du, S. Deckoff-Jones, J. Hu, Y. Zhang, Y. Pan, and C. Rios, "Structurally and morphologically engineered chalcogenide materials for optical and photonic devices," *J. Opt. Microsyst.* **1**, 013502 (2021).

[18] G. Yang, X. Zhang, J. Ren, Y. Yunxia, G. Chen, H. Ma, and J. L. Adam, "Glass formation and properties of chalcogenides in a $GeSe_2-As_2Se_3-PbSe$ system," *J. Am. Ceram. Soc.* **90**, 1500 (2007).

[19] L. Sisken, M. Kang, J. M. Veras, C. Smith, A. Buff, A. Yadav, D. McClane, C. Blanco, C. Rivero-Baleine, T. S. Mayer, and K. Richardson, "Infrared glass ceramics with multi-dispersion and gradient refractive index attributes," *Adv. Funct. Mater.* **29**, 1902217 (2019).

[20] M. Kang, I. Martin, R. Sharma, C. Blanco, S. Antonov, T. J. Prosa, D. J. Larson, H. Francois-Saint-Cyr, and K. A. Richardson, "Unveiling true 3-D nanoscale microstructural evolution in chalcogenide nanocomposites: a roadmap for advanced infrared functionality," *Adv. Opt. Mater.* **9**, 2002092 (2021). 100